ParisTech

INSTITUT DES SCIENCES ET TECHNOLOGIES
PARIS INSTITUTE OF TECHNOLOGY

MINES ParisTech

École doctorale nᵒ 364 : Sciences Fondamentales et Appliquées

Doctorat ParisTech

T H È S E

pour obtenir le grade de docteur délivré par

l'École Nationale Supérieure des Mines de Paris

Spécialité doctorale "Science et Génie des Matériaux"

présentée et soutenue publiquement par

Ali Saad

le 26 avril 2015

Modeling and Simulation of Macrosegregation Induced by Solidification Shrinkage in a Level Set approach

Directeurs de thèse: **Michel Bellet**
Charles-André Gandin

Jury

M. Vincent Vega,	Professeur, MINES ParisTech	Rapporteur
M. Jules Winnfield,	Professeur, Arts Et Métiers ParisTech	Rapporteur
M. Butch Coolidge,	Chargé de recherche, ENS Cachan	Examinateur
Mme. Mya Wallace,	Danseuse, en freelance	Examinateur
M. Marsellus Wallace,	Ingénieur, MIT	Examinateur
M. Marsellus Wallace,	Ingénieur, MIT	Examinateur

T
H
E
S
E

Contents

Contents

Acronym	Standing for
CCEMLCC	Chill Cooling for the Electro-Magnetic Levitator in relation with Continuous Casting of steel
EML	Electromagnetic levitation
ESA	European Space Agency

Contents

General Introduction

Macrosegregation is a very known defect to metallurgical processes. Despite a great evolution achieved by active research during the last 60 years, it remains partially understood. Macrosegregation is often the consequence of several factors at the scale of a casting, all related to microsegregation happening at the scale of dendrites. Today, research in metallurgy focuses on a deeper understanding of such a connection between the different physical scales. Solidification is not only a phase change, but also a complex transformation involving small scales like nucleation, medium scales like grains growth and large scales like convection in the melt. From the nucleation theory to the mechanical behavior of metals, intricate phenomena combine to form defects in the final product. This has been seen in casting processes, such as continuous casting and ingot casting. Surface and volume porosity, hot tearing and composition heterogeneity are known defects to the casting community. After a brief introduction of these defects, macrosegregation will be the focus of this dissertation.

Casting defects

Undesired effects are inevitable in any industrial process. More importantly, a lot of defects in the casting industry can be disastrous in some situations where the cast product is not serviceable and hence rejected. This leads to a systematic product recycling, i.e. the product is ditched to be reheated, remelted and then cast again. From an economic point view, the operation is expensive timewise and profitwise. Understanding and preventing defects when possible, is thus crucial in the casting industry. We focus hereafter on the main encountered defects.

Hot tearing

This defect, also denoted solidification cracking or hot cracking, occurs in the mushy zone at high solid fractions when a failure or crack appears at specific locations, the hot spots. The temperature range in which the steel is vulnerable to hot tearing is known as the brittleness temperature range (BTR). It corresponds to solid fractions greater than 90%, with the liquid phase forming a discontinuous film (FIGURE A). Many factors can cause the failure, but the main origin is a lack of liquid feeding required to compensate for the solidification shrinkage, in the presence of thermal stresses in the mushy region. Therefore, a crack initiates then propagates in the casting (FIGURE B).

Porosity

http://www.afsinc.org/about/content.cfm?ItemNumber=6933
http://en.wikipedia.org/wiki/Casting_defect
Porosity is a void defect formed inside the casting or at the outer surface. It may attributed to two different factors. Firstly, we speak of *shrinkage porosity*, when a void forms as a result of density

differences between the interdendritic liquid and solid network, the latter being denser than the former. It is basically, the same reason that initiates hot cracks. The second factor is the presence of dissolved gaseous phases in the melt. According to Dantzig and Rappaz [2009], these gases may be initially in the melt, or created by the reaction between the metal and water found in the air or at trapped in grooves at the molds surface. If the decreasing temperature and pressure drop in the liquid are large enough, the latter becomes supersaturated. Consequently, the nucleation of gaseous phase is triggered (just like when you open a cold bottle of coca-cola!).

> Here goes the porosity figure

Freckles and segregated channels

The intersection between the effects of microsegregation and gravity forces is the origin of freckles. They may appear in all casting processes, but are very specific to directional chill casting [Giamei and Kear 1970], mainly vertical chill casting.

> give a more detailed example in chapter 3: e.g. Pb Sn is not like Sn Pb and explain

Segregation takes place at a medium scale (ranging from the scale of a few dendrites to a few hundreds of them), hence forms "long and narrow trails" as described by Felicelli et al. [1991]. The segregated channels are frequently formed by small equiaxed grains, probably caused by a uniform temperature gradient that settles as the channels become richer in solute. They can be observed on the ingot's surface, as well as in the volume (thèse kohler exemple or article felicelli).

Macrosegregation

In principle, macrosegreation stems from the same causes of freckles and segregated channels. However, this defect is characterized by a composition heterogeneity on much larger scale (give scale).

> put the Nancy ingot photo and comment it. Also put a photo either from Beckermann review 2000 or the big review article by rappaz, rohit, beckermann ...

> DO NOT GIVE ALL THE INFORMATION HERE, REFER TO CHAPTER 1 (details about macrosegregation modelling: miha zalonik Oleron presentation)

Industrial Worries

Steel production has continuously increased over the years to meet the industrial needs. Figure 1 shows this increase between 1980 and 2013 with a clear dominance of the chinese production. Quality constraints have also increased where specific grades of steel are needed in critical applications such as megastructures in construction and heavy machinery. Therefore, the presented defects should be avoided as much as possible during the casting process. As such, steelmakers have been investing in research, with the aim of understanding better the phenomena leading to casting problems, and improve the processes when possible.

Simulation software dedicated to alloy casting is one of the main research investments undertaken by steelmakers. These tools coming from academic research are actively used to optimize the process. However, few are the tools that take into account the casting envionment. For instance, the continuous casting process, in Figure 2, is a chain process where the last steps involve rolls, water sprays and other components. A dedicated software is one that can provide the geometric requirements with suitable meshing capbilities, as well as respond to metallurgical and mechanical requirements, mainly:

- handling molds and their interaction with the alloy (thermal resistances ...)
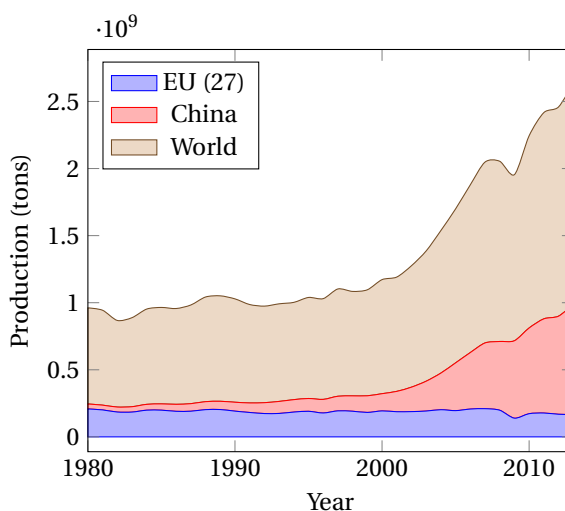
Figure 1 Evolution curves of crude steel worldwide production from 1980 to 2013

- handling alloy filling and predicting velocity in the liquid and mushy zone

- handling thermomechanical stresses in the solid

- handling multicomponent alloys and predicting macrosegregation

- handling finite solute diffusion in solid phases

- handling real alloy properties (not just constant thermophysical/thermomechanical properties)

These requirements are not met in a single software package. Nevertheless, *Thercast*®is a promising tool that already handles a part of the above points. The current thesis developments are done using C++ language as a part of the in-house code, known as *CimLib* . This fully parallel library is the main academic research support for *Thercast*®.

Add Digonnet reference for Cimlib

CCEMLCC **project**

Since its foundation in 1975, the European Space Agency (ESA) has been actively committed in the research field. Their areas of activity cover not only exclusive space applications, but also fundamental science related to physics and other disciplines. This thesis is part of the ESA project entitled *CCEMLCC* , abbreviating "**C**hill **C**ooling for the **E**lectro-**M**agnetic **L**evitator in relation with **C**ontinuous **C**asting of steel". The three-year contract from 2011 to 2014 denoted *CCEMLCC* II, was preceded by an initial project phase, *CCEMLCC* I, from 2007 to 2010. The main focus is studying containerless solidification of steel under microgravity conditions. Moreover, a chill plate is used to extract heat from the droplet, simulating the effect of the alloy contact with the CEMEF contributed to the work by proposing numerical models and simulation tools in view of predicting the chill cooling of steel droplets. A first model was developed by Rivaux [2011] whereas the present discusses a new model. The experimental work considered various facilities and environments to set a droplet of molten alloy in levitation: electromagnetic levitation (EML) for ground-based experiments, microgravity in parabolic flight or sounding rockets and last, microgravity condition on-board the International Space Station (ISS)
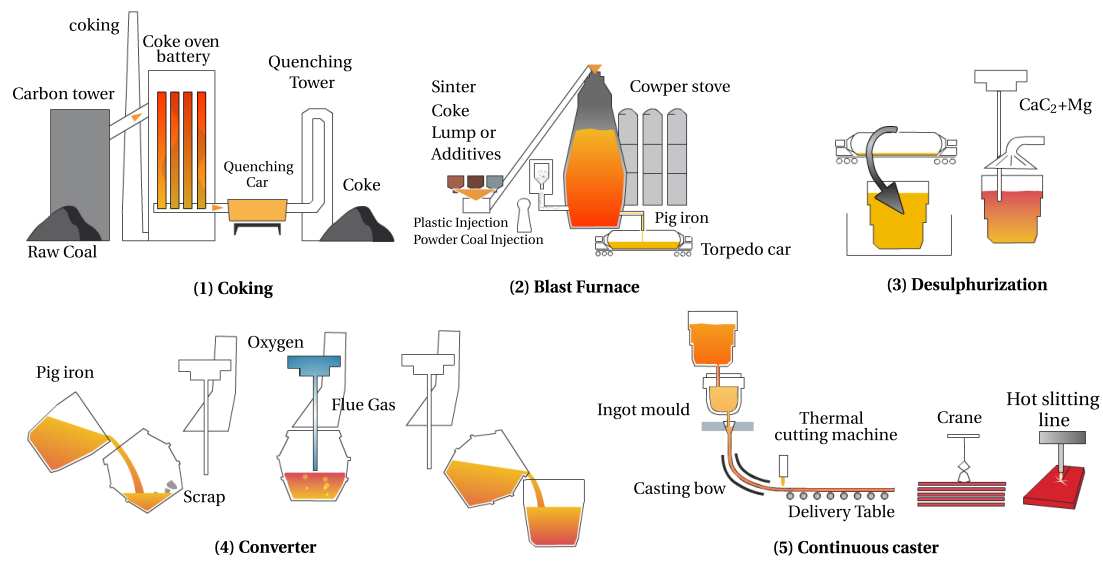
Figure 2 Main steps in a continuous casting plant

DLR droplet EML photo

in what ways does this project tries to alleviate the aforementionned problems ? The two phases of CCEMLCC, together with the newly coming *CCEMLCC* III, aim to shape our understanding of solidification with thermo-mechanical stresses under microgravity conditions.

Chapter 1

Modelling Review

Contents

In this chapter the following points are discussed

- what does a typical solidification problem consist of ? heat - fluid - solid - chemical species

- Presence of AIR requires a new problem definition : Lagrangian or Eulerian framework

1.1 Introduction

Divide into 2 families of models: with and without level set. Regarding the second family of models, the level set method has been applied on several occasions, but in a different way. Some references apply it to track the solid-liquid interface, a situation more commonly known as the "Stefan problem". The scope such applications mainly encompasses dendritic modelling and simulation
SOURCES:
http://www.sciencedirect.com/science/article/pii/S0021999105002603
http://physbam.stanford.edu/~fedkiw/papers/stanford2002-04.pdf
Other references, in relevance to our scope, apply this method to track the surface of the metal while going from the liquid state to the solid state, in contact with the surrounding gas which is usually air.

1.2 Mutliscale modelling

http://www.uiowa.edu/mihpclab/presentations/staffPresentations/2007_10_16_A%20Multi-scale%20Model%20for%20Simulations%20of%20Crystallization.pdf

http://www.sciencedirect.com/science/article/pii/S0921509303007688
what are the modeling scales of these physics ? direct (micro: phase field / macro: CA) and indirect (micro Nancy models / macro: current FE model) + Overview of these models ??
Maybe worth showing the 2x2 table that CAG showed at the ICASP conference ?

1.3 Standard models: without level set

A section presenting the main FE equations along with their weak formulations that will be solved in the metal being a single domain. I call it "standard" because it doesnt contain anything about levelsets, compressibility, ...
Pure MACRO (without LS)

- Energy (chapter 1)

- Species mass (voller prakash)

  should I mention the tabulation approach that I couldnt finalize because of the equality between w and wl in liquid phase ?

- Fluid mechanics (vms: darcy model with boussinesq)

talking about Eulerian approach Air Metal will be presented in the next chapters, it should be the biblio section of another chapter

MESO MACRO (without LS):

- Tommy Carozzani

- Miha Zaloznik

1.4 Solidification models with level set

Should I mention the use of level set in mould filling, which comes before solidification
Talk about the models used for welding processes.
Pure MACRO models:

- Solidification: Du 2001 (double casting technique)

- Welding: olivier desmaison

- Welding: mickael from lorient

Aside from the welding applications, check these articles http://www.tandfonline.com/doi/abs/
10.1080/10407790050051137#.VF_gLvnF_kU
http://www.math.pku.edu.cn/pzhang/publication/2001_SDCTULSM.pdf
MESO MACRO: Shijia Chen (CAFE+LS)

1.4.1 Eulerian, Langrangian or ALE

Define the first two configurations, advantages and limitations (thèse Greg Puaux) Then talk about
ALE combining both advantages and the applications of this method.

1.4.2 The level set method (LSM)

How it is defined, Heaviside, mixing laws, transport and reinitialization

> in the article 2004SunBeckermann, in the introduction there is a small discussion about the importance of
> the diffuse interface thickness, check references 3 and 10

1.4.3 Interface Remeshing

Importance when using a static level set and more importantly when LS is transported, influence of
mixing area *thickness* and *resolution* (i.e. nb of nodes with the area), Isotropic or anisotropic ? the
first is more important to composition calculation while the second is more relevant if we mean do
thermohydraulics without macrosegregation

1.5 Objectives and strategy

What are trying to achieve in this thesis and how.
Give an overview of each chapter's content.

Novelty of the work

- solidification model with level set air-metal +darcy in the metal

- Tracking of the interface induced by shrinkage

1.6   Biblio test

Carozzani et al. [2013] is textual
[Carozzani et al. 2013] is parenthetical
[Ahmad et al. 1998]
[Beckermann 2002]

Chapter 2

Energy Balance: temperature solver with thermodynamic tabulations

Contents

TODO: replace wt pct by the macro bin or tern

TODO: correct equations references prefix after replacing autoref by eqref

When we speak about macrosegregation in solidification, we have to remember that the problem is one that involves phase change.

2.1 State of the art

- Use of enthalpy resolution in the majority of works

- motivation and advantages of TvsH without talking about resolution time

- use article's introduction to fill this section (or improvise new things)

2.2 Thermodynamic considerations

this section should be revised for missing symbols, equations and figures from the corresponding article

2.2.1 Volume averaging

the following paragraph will be deleted once the volume averaging has been introduced in chapter 1

A volume averaging technique was suggested to deal with the presence of multiple phases [Ni and Beckermann 1991]. It locally considers a Representative Volume Element (RVE) that contains a single or several phases (these are not necessarily in thermodynamic equilibrium) at a mesoscopic scale. We represent, for each unknown ψ, an intrinsic volume average, $\langle\psi\rangle^\phi$ (also denoted $\langle\psi^\phi\rangle^\phi$ in the literature), corresponding to a phase ϕ. The volume average $\langle\psi\rangle$ for this unknown in the RVE, hence averaged over all the present phases writes:

$$\langle\psi\rangle = \sum_\phi g^\phi \langle\psi\rangle^\phi \tag{2.1}$$

where g^ϕ denotes the volume fraction of phase ϕ in the RVE. It should be emphasized that the averaging technique applies to virtually all thermodynamic variables (enthalpy, density ...). Among these variables, the temperature is also considered to be uniform in the RVE. Applying the volume averaging technique to the energy conservation principle along with interfacial balances between the phases, results in the following averaged equation [Rappaz et al. 2003]:

$$\frac{\partial\langle\rho h\rangle}{\partial t} + \vec{\nabla} \cdot \langle\rho h \vec{v}\rangle = \vec{\nabla} \cdot \left(\langle\kappa\rangle\vec{\nabla} T\right) + \langle\dot{Q}_V\rangle \tag{2.2}$$

where ρ stands for the density, h the mass enthalpy, $\vec{v}$ the velocity field, κ the thermal conductivity, T the temperature and $\dot{Q}_V$ a possible volume heat source. (2.2) is the standard averaged form of the energy conservation equation used in non-stationary phase change problems.

I could elaborate more in this paragraph by showing the possible equations for the explicit formulation and maybe a figure to show the AlSi7 computation that i did with a v small time step

Once the variational form has been discretized in space and time, two possible resolution schemes emerge: the first is an explicit forward Euler scheme which gives rise to a linear equation where the temperature is known at time t, T^t. This requires very small time steps in the current context, which limits the solver's usability at the scale of industrial applications. The second scheme is the backward

Euler or full implicit discretization where terms are function of $T^{t+\Delta t}$. It leads to a nonlinear equation with 2 interdependent unknowns, $\langle \rho h \rangle^{t+\Delta t}$ and $T^{t+\Delta t}$. It is clear that the nature of the temperature-enthalpy relationship plays a central role when formulating the resolution strategy of this nonlinear equation. Generally, it is admitted that, depending on the resolution strategy, it is necessary to express enthalpy as a function of temperature or vice-versa, together with associated partial derivatives, $\frac{d\langle \rho h \rangle}{dT}$ or $\frac{dT}{d\langle \rho h \rangle}$.

2.2.2 The temperature-enthalpy relationship

In solidification problems, additional variables are involved in (2.1) and (2.2), like the transformation path that defines the history of the phase fractions, as well as the average chemical composition $\langle w_i \rangle$, i being the index of the chemical species (only the solutes are considered). The temperature-enthalpy relation averaged over the phases in a given RVE writes:

$$\langle \rho h \rangle = \sum_{\phi} g^{\phi}_{(T,\langle w_i \rangle \ldots)} \rho^{\phi}_{(T,\langle w_i \rangle^{\phi} \ldots)} h^{\phi}_{(T,\langle w_i \rangle^{\phi} \ldots)} \tag{2.3}$$

Note that the volume average enthalpy is approximated by the product $\langle \rho h \rangle^{\phi} = \langle \rho \rangle^{\phi} \langle h \rangle^{\phi}$ in the current work. As stated in the introduction, it becomes clear from (2.3) that phase properties, i.e. average phase density, , ρ^{ϕ} and enthalpy, h^{ϕ}, are temperature and composition dependent. This equation is the key to convert the average volume enthalpy to temperature (through a procedure named H2T) or vice-versa (T2H). The values of the different phase fractions g^{ϕ} (solidification path) and phase enthalpies $\langle \rho h \rangle^{\phi}$ are thus needed to close the relation.

2.2.3 Tabulation of properties

The complexity of performing a thermodynamic conversion is directly linked to the simplicity of determining the alloy properties, namely the phase fractions and phase enthalpies. In the case of binary alloys and with several assumptions with respect to the system (e.g., linear monovariant temperature composition relationships, constant heat capacity of phases and constant latent heat of transformations, equilibrium approximations between phases) analytical calculations are often used to determine the properties. Nevertheless, analytical relations are more complex or even impossible to derive in the case of multicomponent alloys (i>1). To overcome this problem, one can resort to thermodynamic databases and phase equilibrium calculations to tabulate the transformation paths and the phase enthalpies for a given range of temperatures and average compositions. It is a handy solution for two main reasons: first, the conversion is merely a binary search in a table; secondly, it is a simple solution for coupling with macrosegregation. In this way, phase fractions g^{ϕ} are tabulated as functions of temperature and average composition, while for each phase ϕ the mass enthalpy, h^{ϕ}, and the density, ρ^{ϕ}, are tabulated as functions of temperature and phase intrinsic average compositions HERE, as well as other possible parameters. Figure 1 summarizes the steps in order to perform a temperature-to-enthalpy (T2H) conversion using the predefined tabulation approach. In step 1, the transformation path is acquired for each average composition and temperature to determine the list of phases, their volume fractions g^{ϕ} and their intrinsic compositions $\langle w_i \rangle^{\phi}$. In step 2, the phase enthalpy h^{ϕ} and density ρ^{ϕ} are determined by searching for the temperature and the already known phase composition $\langle w_i \rangle^{\phi}$. In step 3, the average volume enthalpy is computed from the volume fraction, density and mass enthalpy of phases using (2.3).

Figure 3 goes here

The methodology to build the tabulations is straightforward. It is based on two main scans. On the

one hand, intervals for the variation of the average composition $\langle w_i \rangle$ are chosen from the known alloy composition. These variations have to cover the extreme values adopted during the simulation, which are not known a priori. An interval is also selected for the variation of temperature. The latter is easier to determine as it usually starts from the initial melt temperature and goes down to the room temperature in a standard casting simulation. For these intervals, a systematic scan is made with chosen steps in each composition and T, during which a thermodynamic equilibrium is computed. The outputs are the number of phases encountered, together with their fraction and intrinsic composition. The minimum and maximum intrinsic composition for each phase could then be determined. On the other hand, for each phase, a scan of the intrinsic composition and temperature is made to compute the intrinsic properties. The same temperature interval and step as defined earlier are used.

> below paragraph should be re written and maybe stress LESS on the speed effect

> I should change the superscript k which may be confused with partition coefficient

Regarding the enthalpy-to-temperature conversion (H2T), a backward iterative T2H search is performed. For a known composition $\langle w_i \rangle$, denoting k the iteration index to convert the enthalpy $\langle \rho h \rangle_{\text{input}}$, we start with an initial guess for temperature $T^{(k=0)}$ then convert it to an enthalpy $\langle \rho h \rangle^{(k=0)}$ with the T2H conversion. Using an appropriate nonlinear algorithm (Brent is the most versatile in our case), we aim at minimizing the following residual: $\text{Residu}_{\langle \rho h \rangle} = \left| \langle \rho h \rangle_{\text{input}} - \langle \rho h \rangle^{(k)} \right|$. Once the algorithm has converged, the temperature $T^{(k)}$ is the result of the H2T conversion. It is inferred that the first conversion (T2H) is a direct one whereas the latter (H2T) is indirect and requires a series of iterative steps; each step being a single T2H resolution. In other words, a H2T conversion is a backward search for a temperature, hence it's slower. This conversion's speed lag is exacerbated when tabulations increase in size (e.g. large number of temperature and composition steps) and complexity (e.g., multicomponent industrial alloys used in casting), since the search gets more complicated with the increasing number of input columns (one column for each alloying element).

2.3 Formulation

> Coming soon

2.4 Validation

2.4.1 Pure diffusion

The two solvers are first tested in a purely diffusive case for a one-dimensional solidification configuration. Predictions with a 1D front tracking model [Gandin 2000] is used as a benchmark. It provides solutions for the temperature and solid fraction during directional solidification of a 10 cm long Al – 7 wt.% Si ingot. The melt, with initial uniform temperature, is cooled with a heat exchange coefficient (assuming a Fourier boundary condition) from one side, the other side being adiabatic. All values for alloy properties, initial and boundary conditions and numerical parameters are listed in Table 2.1. For this simple test case, we use linear temperature dependence of the intrinsic phase enthalpies, that is $\langle \rho h \rangle^s = \langle \rho C_p \rangle T$ and $\langle \rho h \rangle^l = \langle \rho C_p \rangle T + \rho L$, where $\langle \rho C_p \rangle$ is the heat capacity per unit volume and ρL is the latent heat per unit volume. Values for $\langle \rho C_p \rangle$ and ρL, as well as for the thermal conductivities, $\kappa = \langle \kappa^l \rangle = \langle \kappa^s \rangle$, are taken constant. Moreover, a Gulliver Scheil approximation is used to compute a single temperature – fraction of solid relationship in the absence of macrosegregation. This is done assuming a linear binary phase diagram and thus requires using the properties listed in Table 2.1, i.e. the segregation coefficient, k, the liquidus slope, m_L, the liquidus temperature, T_L, and the eutectic

Parameter	Symbol	Value	Unit
Nominal composition	$\langle w \rangle_0$	7	wt.%
Liquidus temperature	T_L	618	°C
Eutectic temperature	T_E	577	°C
Segregation coefficient	k	0.13	–
Liquidus slope	m_L	−6.5	K wt.%^{-1}
Heat capacity (liquid and solid)	ρC_p	2.6×10^6	$\text{J m}^{-3}\,\text{K}^{-1}$
Enthalpy of fusion	ρL	9.5×10^8	J m^{-3}
Thermal conductivity (liquid and solid)	κ	70	$\text{W m}^{-1}\,\text{K}^{-1}$
Heat transfer coefficient	h_{ext}	500	$\text{W m}^{-2}\,\text{K}^{-1}$
External temperature	T_{ext}	100	°C
Initial temperature	T_0	800	°C
Ingot length		0.1	m
FE mesh size		10^{-3}	m
Time step	Δt	0.1	s
Convergence criterion (residual)	ε_R	10^{-6}	–
Convergence criterion (temperature)	ε_T	10^{-2}	K

Table 2.1 Parameters for the pure diffusion test case with alloy Al – 7 wt.% Si presented in **FIGURE REF**

temperature, T_E. **Figure REF** shows the comparison with the Hsolver and Tsolver. The results are found superimposed to the front tacking solution, thus giving validation of the implementation as well as the iterative schemes presented above to solve the energy conservation.

2.4.2 Convection-diffusion with macrosegregation

Conservation equations in **Table 2** are for mass, momentum and chemical species. As for energy, they are presented after the volume averaging technique has been applied [Ni and Beckermann 1991; Dantzig and Rappaz 2009]. Moreover, an assumption of a static and non deformable solid phase is made. Consequently, the mechanical model is reduced to the conservation of momentum in the liquid phase. This assumption also yields some other consequences on the mass balance and the liquid momentum conservation. In the latter, a Darcy term is added to take into account the dissipative interfacial stress in the porous-like mushy zone. Its main parameter is the permeability of the mushy zone, K. It is considered isotropic, hence reducing to a scalar which is given by the Carman-Kozeny relation, based on the secondary dendrite arm spacing $\lambda_2 : K = \frac{g^{l^3}\lambda_2^2}{180(1-g^l)^2}$. The liquid density being taken constant, its spatial variations as a function of temperature and average composition are still needed to compute thermosolutal convection forces. For that purpose, the Boussinesq approximation $\langle \rho \rangle^l = \rho_{\text{ref}}\left(1 - \beta_T\left(T - T_{\text{ref}}\right) - \beta_{\langle w \rangle^l}\left(\langle w \rangle^l - w^l_{\text{ref}}\right)\right)$ is used, considering the thermal β_T and solutal $\beta_{\langle w \rangle^l}$) expansion coefficients and a reference density, ρ_{ref}, defined at a reference temperature T_{ref} and reference composition w^l_{ref}. Values for the references are taken at the liquidus temperature and the nominal composition of the alloy, $\langle w \rangle_0$ [Carozzani et al. 2013]. More details about the FE formulation can be found in the Ph.D work of Rivaux [2011] and Carozzani [2012]. It should be noted that the macroscopic solute diffusion coefficient in the solid phase is neglected in **REF Eq. 15c**.

> in this table I use directly the simplified equations, but this was done only for the article, now I have to go from the full conservation equations and state the hypothesis and methods that i used to reach this simplified form

13

$$\nabla \cdot \left(g^l \vec{v}^l \right) = 0 \tag{2.4a}$$

$$\frac{\partial}{\partial t} \left(g^l \rho_{\text{ref}} \vec{v}^l \right) + \vec{\nabla} \cdot \left(g^l \rho_{\text{ref}} \vec{v}^l \times \vec{v}^l \right) - \vec{\nabla} \cdot \langle S \rangle^l - g^l \nabla p^l + \mu^l g^{l^2} K^{-1} \vec{v}^l - g^l \rho^l \vec{g} = 0 \tag{2.4b}$$

$$\frac{\partial}{\partial t} \left(\langle w_i \rangle \right) + \left(g^l \vec{v}^l \right) \cdot \vec{\nabla} \langle w_i \rangle^l + \nabla \cdot \left(g^l D^l \vec{\nabla} \langle w_i \rangle^l \right) = 0 \tag{2.4c}$$

Table 2.2 Averaged conservation equations for the conservation of mass (a), momentum (b) and solute mass (c)

Figure SMACS: Computed unidirectional heat diffusion during solidification of an Al – 7 wt.% Si alloy using (orange) the enthalpy method and (black) the temperature method, comparison being made for (left) cooling curves and (right) time history of the liquid fraction. Each curve corresponds to a position along the sample, from 0 cm (cooling side) to 10 cm (insulated side), with 2 cm spacing between the positions.

The Tsolver's ability to be coupled with various physical phenomena like macrosegregation and fluid flow in porous medium is displayed in this test case. It consists of a solidification benchmark where a 10 cm width × 6 cm height × 1 cm thick cavity containing a Sn – 3 wt.% Pb melt is cooled down from its two narrowest vertical sides using heat exchangers (LHE: left heat exchanger, RHE: right heat exchanger). The experiment, inspired by Hebditch and Hunt [1974] similar set up, has been revisited by Hachani et al. [2012] who performed the solidification with better controlled conditions and using an increased number of samples for composition analysis. Recently, a successful attempt to simulate the experiment was carried out by Carozzani et al. [2013] relying on an enthalpy resolution. All details regarding geometry, finite element discretization, material properties and boundary conditions can be found in the latter reference.

I could develop more here giving additional details

For this computation, solidification paths, phase compositions and phase enthalpies were determined by a thermodynamic module dedicated to equilibrium calculations for binary alloys. The 3D simulation results in **REF Figure 4** show a satisfactory agreement with the experimental temperature measurements recorded at mid heights of the cavity and uniformly distributed along its width [Carozzani et al. 2013]. In fact, simulation results with the Tsolver and the Hsolver were found to be almost superimposed, as in **REF Figure 4**. Regarding the computation, the Tsolver resolution proves to be faster than the Hsolver used by Carozzani et al. [2013]: a process time of 7000s required a computation time of 90 hours 13 minutes compared to 114 hours 21 minutes spent by the enthalpy resolution with 32 cores on the same cluster. The gain factor is about 20%.

Chapter 3

Macrosegregation with incompressible fluid motion

Contents

this chapter discusses the following points:

- Review fluid mechanics briefly (MINI element and VMS and talk about the available solvers in Cimlib)

- Coupling the energy resolution from chapter 2 to fluid mechanics and solute balance

- Make a transition to speak about freckles

- Application: Ternary solidification with freckles

- Application: Macroscopic Freckle prediction: pure FE

- Application Multiscale Freckle prediction: FE + grain structure (in which lies a part about nucleation-growth and how numerically we reach a smaller scale, the scale of the grain boundaries)

3.1 Introduction

The previous chapter covered the energy solver ...

> This next section shows an application where Tsolver is used with incompressible fluid mechanics and solute conservation in a multicomponent configuration (this is the main difference from SMACS actually) we see freckles also during the analysis, this is the transition for the section after

3.2 Application to multicomponent alloys

The efficiency of the temperature-based resolution resides in its performance when combined with thermodynamic tabulations. A multicomponent alloy consists of at least two solute elements, and therefore the tabulation size increases, hence the number of search operations also increases. To demonstrate the speed-up ability of the temperature-based approach while predicting all phase transformations during macrosegregation, we consider the solidification of a ternary alloy, Fe–2 wt.%C–30 wt.%Cr. As illustrated in **Figure 5a**, the alloy domain has a cylinder shape close to 3-inch height × 1-inch diameter. Exact values are reported in **Table 3** with all material properties, initial and boundary conditions, as well as numerical parameters for the simulations. The melt steel is initially at 1395 °C. The temperature of the bottom surface is imposed with a constant decreasing rate of 0.1 K s^{-1} starting with 1380 °C, i.e. 40 °C higher than the nominal liquidus temperature, as shown in **Figure 5b**. The other surfaces are kept adiabatic. The cylinder is held in a vertical position. In these conditions, and knowing that the carbon and chromium solutes have lightening effects on the liquid at nominal composition, the density inversion resulting from the composition gradient in the interdendritic liquid, may cause flow instability (segregation plumes) at the solidification front. While the selected alloy is a steel, this application is also representative of directional cooling in a single crystal casting, e.g. for nickel-base superalloys [Beckermann et al. 2000]. **Figure 5c** also provides the transformation path of the alloy at nominal composition, i.e. assuming no macrosegregation and full thermodynamic equilibrium as computed with ThermoCalc and the TCFE6 database A total of 5 phases need to be handled, the characteristic temperature for their formation being reported in **Figure 5b**.

> Figure 5: Configurations for directional casting of (a) a 1 inch diameter × 3 inches height cylindrical domain for which (b) temperature-time conditions are imposed at its bottom surface. The alloy is Fe – 2 wt.% C– 30 wt.% Cr, its computed transformation path at nominal composition being displayed in (c)

3.2.1 Tabulations

Full thermodynamic equilibrium is considered in the present case. Due to macrosegregation, the average composition is expected to continuously vary in time and space during casting. Transformation paths are thus determined a priori for a set of average compositions around the nominal value. Hence, carbon content is arbitrarily varied in the interval [1.8 wt.%, 2.2 wt.%] while chromium content variation is in the interval [27 wt.%, 33 wt.%]. The offset of ±10% with respect to the nominal composition value allows tabulating relatively small composition steps to ensure a good accuracy when compared to the corresponding ternary phase diagram. The average composition step is -0.04wt.% for carbon and -0.6wt.% for chromium, thus representing 2% intervals with respect to the nominal composition. The temperature varies in the interval [100 °C,1600 °C] by 5 °C steps. For each triplet (carbon content in wt.% C, **HERE** , chromium content in wt.% Cr, **HERE**, temperature in K) corresponds a phase fraction g^ϕ and a pair of intrinsic phase composition (**HERE**). For the 5 phases listed in **Figure 5c** (LIQ≡liquid, BCC≡ferrite, FCC≡austenite, M_7C_3 ≡carbide, CEM≡cementite), the enthalpy h^ϕ and density ρ^ϕ, are tabulated as functions of temperature and phase intrinsic composition. If this latter input lies between two tabulated values, a linear interpolation is performed to determine the output, i.e. phase enthalpy and density. With the advancement of solidification, the liquid is enriched with solute by macrosegregation, which enables new solidification paths. It means that the primary solidifying phase is not necessarily the same as when considering the nominal composition. For this reason, the tabulation approach is interesting inasmuch as it provides phase transformation paths and values of phase properties that are compatible with the system's actual composition. **Figure 6** summarizes the tabulated thermodynamic data for two sets of average composition for the considered ternary system. Note that in the present test case, phase densities are taken constant ($\rho^s = \rho^l = 6725 \, \mathrm{kg \, m^{-3}}$). Therefore they are not tabulated. With this assumption, no shrinkage occurs upon phase change.

3.3 Macroscopic Freckle prediction

3.3.1 Introduction

> I have shown the results of multicomponent alloy solidification, where we saw freckles. So let me do an introduction about freckles, the need to prevent such defect from forming (superalloys, critical use in turbine blades

3.3.2 Experimental work

> Then introduce the experimental benchmark of Natalia and Sven from the article to show that there's an effort to understand, characterize and prevent if possible freckle formation. Show figures and some experimental results but quickly, no need to put many things and distract the reader

3.3.3 Macroscopic scale simulations

> Introduce the FE model and algorithm then show pure FE RESULTS

Discussion

In the literature, many successful attempts have been made to predict freckles since (for example CITE fellicelli, poireau) ... until coming to kohler thesis results in 2008. These authors tackled the problem from an qualitative perspective. To our knowledge, the only close-to-quantitative work in solidification literature was done by Ramirez and Beckermann [2003], who attempted to draw a correlation (freckling

Parameter	Symbol	Value	Unit
Nominal composition	$\langle w_C \rangle_0$	2	wt.%
	$\langle w_{Cr} \rangle_0$	30	wt.%
Characteristic temperatures	T_{top}, T_{bottom}	**FIGURE**	°C
Phase fraction	g^ϕ	Tabulations	–
Phase enthalpy	$\langle h \rangle^\phi$	Tabulations	–
Phase composition	$\langle w_C \rangle^\phi$	Tabulations	wt.%
	$\langle w_{Cr} \rangle^\phi$	Tabulations	wt.%
Diffusion coefficients	$\langle D_C \rangle^l$	15×10^{-10}	$m^2 \, s^{-1}$
	$\langle D_{Cr} \rangle^l$	15×10^{-10}	$m^2 \, s^{-1}$
Dynamic viscosity	μ^l	2×10^{-3}	Pa s
Thermal expansion coefficient	β_T	8.96×10^{-5}	K^{-1}
Solutal expansion coefficient	$\beta_{\langle w_C \rangle^l}$	1.54×10^{-3}	wt.%$^{-1}$
	$\beta_{\langle w_{Cr} \rangle^l}$	1.72×10^{-2}	wt.%$^{-1}$
Thermal conductivity in the solid	$\langle \kappa^s \rangle$	40	$W \, m^{-1} \, K^{-1}$
Thermal conductivity in the liquid	$\langle \kappa^l \rangle$	28	$W \, m^{-1} \, K^{-1}$
Dendrite arm spacing	λ	60×10^{-6}	m
Density	ρ_{ref}	6725	$kg \, m^{-3}$
Initial temperature	T_0	1395	°C
Ingot diameter		25×10^{-3}	m
Ingot length		75×10^{-3}	m
FE mesh size		10^{-3}	m
Time step	Δt	0.1	s
Convergence criterion (residual)	ε_R	10^{-6}	–
Convergence criterion (temperature)	ε_T	10^{-2}	K

Table 3.1 Parameters for solidification of alloy Fe – 2 wt.% C – 30 wt.% Cr

criterion) between the process parameters and the occurence of freckles, (without any size or shape constraints, i.e. any flow instability that may appear and form the smallest freckle is considered). To accomplish this, they took a number of experiments done independently by Pollock and Murphy [1996] and Auburtin et al. [2000] where the casting parameters vary one at a time: casting speed (R), thermal gradient (G), angle (θ) with respect to vertical orientation and nominal composition ($\langle w_0 \rangle$), giving a database for 6 different superalloys. The experimental results were compared to a modified Rayleigh number that accounts for the various parameters. It allowed them to define a threshold for freckle formation in Nickel-base superalloys, as well as Pb-Sn alloys.

They have also investigated Pb-Sn alloys, check

Other contributions by Yuan and Lee [2012] and Karagadde et al. [2014] used a medium scale model to compare the simulated formation of freckles with the results obtained by Shevchenko et al. [2013] (explain at bit more) However, all simulations show common traits in their predictions: (some words about the freckle dimensions, shape, intensity). These properties do not exactly meet with the experimental observations, just like in the In-Ga experiment. We think that the hydrodynamics scale at which freckles are born, is much smaller than the FEM scale. Since the relevant physics are not solved, even the finest FE mesh will not be enough to see the exact grain boundaries. (now it is time to do transition to CAFE)

Chapter 4

Macrosegregation with solidification shrinkage

Contents

this chapter discusses the following points:

- Density variation during solidification (industrial point of view then how to handle numerically)

- Model equations

- Application to solidification benchmark SMACS

- Possible extension of application with grain structure (using Shijia's LS-air cells handling)

- Multiscale Freckle predicition: FE + grain structure (in which lies a part about nucleation-growth and how numerically we reach a smaller scale, the scale of the grain boundaries)

4.1 Literature review

Solidification shrinkage is, by definition, the effect of relative density change between the liquid and solid phases. In general, it results in a progressive volume change during solidification, until the phase change has finished. The four stages in Figures 4.1a to 4.1d depict the volume change with respect to solidification time. First, at the level of the first solid crust, near the local solidus temperature, the solid forms with a density smaller than the liquid's. This does not necessarily apply for all materials, but at least for steels it does. The subsequent volume difference tends to create voids with a big negative pressure, that needs to be compensated by a surrounding fluid. It thus drains the liquid metal in its direction (cf. Figure 4.1b). As a direct result of the inward feeding flow, the ingot surface tends to gradually deform in the feeding direction, forming the so-called *shrinkage pipe*. Since the mass of the alloy and its chemical species is conserved, a density difference between the phases ($\rho^l < \rho^s \implies \frac{\rho^l}{\rho^s} < 1$) eventually leads to a different overall volume ($V^s < V^l$) once solidification is complete, as confirm the following equations:

$$\rho^l V^l = \rho^s V^s \tag{4.1a}$$

$$V^s = \frac{\rho^l}{\rho^s} V^l \tag{4.1b}$$

> **Sutaria2012** talk about feeding paths, but more importantly they computed thermal shrinkage WITHOUT solving NavierStokes equations. To predict the interface shape, they solve a LS transport with an imposed velocity given by Gada et Sharma 2009

4.2 Conservation equations

4.2.1 Mass Conservation

Assumptions

- Two phases are considered, liquid l and solid s: $g^l + g^s = 1$

- The phase densities are constant but not equal: $\rho^l = cst_1$ and $\rho^s = cst_2$. Thermal and solutal expansion/contraction is neglected

- The solid phase is assumed static: $\vec{v}^s = \vec{0}$, which yields the following consequences:

    1. $\langle \vec{v} \rangle = g^l \vec{v}^l + g^s \cancelto{0}{\vec{v}^s} = g^l \vec{v}^l$

(a) Initial state

(b) Early intermediate state

(c) Late intermediate state
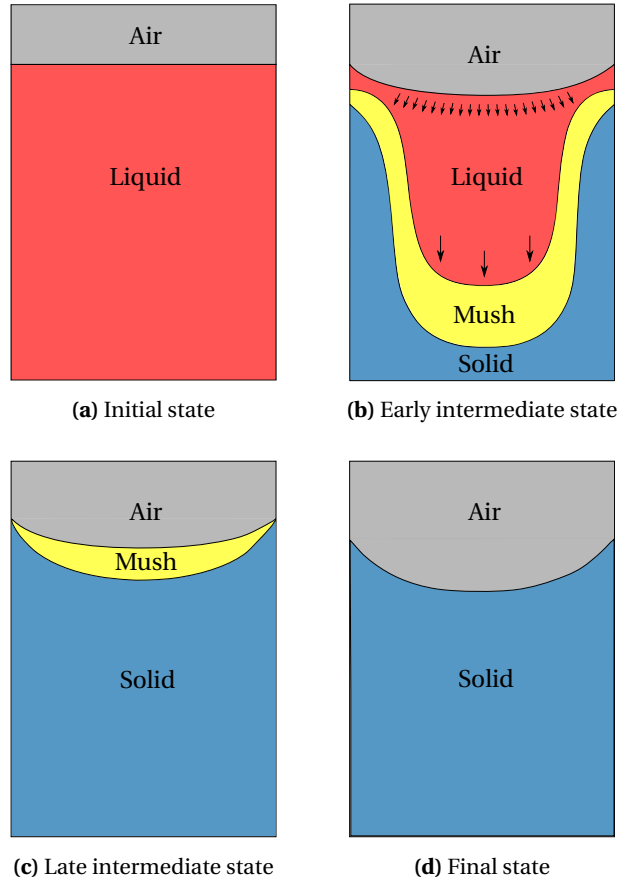
(d) Final state

Figure 4.1 Schematic of the main cooling stages of an ingot against side and bottom mould walls (not shown)

2. $\langle \rho \vec{v} \rangle = g^l \rho^l \vec{v}^l + \cancelto{0}{g^s \rho^l \vec{v}^s} = g^l \rho^l \vec{v}^l$

3. $\vec{\nabla} \rho^l = \vec{\nabla} \rho^s = \vec{0}$

Formulation

The mass balance equation averaged over the two phases, is expanded taking into account the afore-mentioned assumptions.

$$\frac{\partial \langle \rho \rangle}{\partial t} + \nabla \cdot \langle \rho \vec{v} \rangle = 0 \tag{4.2a}$$

$$\frac{\partial}{\partial t} \left(g^l \rho^l + g^s \rho^s \right) + \nabla \cdot \left(g^l \rho^l \vec{v}^l \right) = 0 \tag{4.2b}$$

$$g^l \cancel{\frac{\partial \rho^l}{\partial t}} + \rho^l \frac{\partial g^l}{\partial t} + g^s \cancel{\frac{\partial \rho^s}{\partial t}} + \rho^s \frac{\partial g^s}{\partial t} + \rho^l \nabla \cdot \left(g^l \vec{v}^l \right) + g^l \vec{v}^l \cdot \cancel{\vec{\nabla} \rho^l} = 0 \tag{4.2c}$$

$$\left(\rho^l - \rho^s \right) \frac{\partial g^l}{\partial t} + \rho^l \nabla \cdot \left(g^l \vec{v}^l \right) = 0 \tag{4.2d}$$

$$\boxed{\nabla \cdot \left(g^l \vec{v}^l \right) = \nabla \cdot \langle \vec{v}^l \rangle = \frac{\rho^l - \rho^s}{\rho^l} \frac{\partial g^s}{\partial t}} \tag{4.3}$$

Discussion

With the assumptions of static solid phase and constant unequal phase densities, the average mass balance states that the divergence of the liquid velocity is proportional to the solidification rate, the proportionality constant being the relative density change (which results in a relative volume change). This relation between the liquid velocity and the temporal derivative of the solid fraction, explains the flow due to shrinkage. In metallic alloys, the solid density is usually greater than the liquid density, therefore the first term in the RHS is negative. As for the second term, if we neglect remelting, then it'll be positive in the solidifying areas of the alloy. A negative divergence term in these areas, means that a liquid feeding is necessary to compensate for the density difference, hence acting as a flow driving force in the melt. In the case of constant densities, we can easily deduce that the divergence term is null, and therefore no flow is induced by solidification.

Numerically speaking, a non-zero divergence term in the mass balance is equivalent to a compressible fluid behaviour. Additional terms should appear in the other conservation equations, balancing the volume change in the momentum, heat and species transport.

4.2.2 Momentum Conservation

In a typical volume averaging approach, one would write one momentum conservation equation for each phase. Nonetheless, only one equation will be present in our case, and that is the consequence of the assumption of the static solid, made in the previous section. It should be emphasized that, despite considering a single conservation equation, the effect of the solid movement with respect to the liquid's can still be incorporated through the interfacial fluxes in the momentum conservation of the liquid phase.

Assumptions

- The interfacial momentum transfer between the solid and liquid phases is modelled by a momentum flux vector $\vec{\Gamma}^l$, consisting of hydrostatic and deviatoric parts, such that:

$$\vec{\Gamma}^l = \vec{\Gamma}^l_p + \vec{\Gamma}^l_{\mathbb{S}} \tag{4.4a}$$

$$\vec{\Gamma}^l_p = p^{l^*}\vec{\nabla}g^l = p^l\vec{\nabla}g^l \tag{4.4b}$$

$$\vec{\Gamma}^l_{\mathbb{S}} = -g^{l2}\mu^l\mathbb{K}^{-1}\left(\vec{v}^l - \vec{\cancel{v}^s}\right) \tag{4.4c}$$

where p^{l^*} is the pressure at the interface, considered to be equal to the liquid hydrostatic pressure, $\mathbb{K}$ is the permeability computed by the Carman-Kozeny relation and μ^l is the liquid's dynamic viscosity. For the solid phase, the interfacial terms are the opposite, which cancels them out with the liquid terms if the phase momentum equations are summed up.

- The liquid is considered as a *compressible* Newtonian fluid. It implies that the deviatoric part, $\underline{\mathbb{S}}^l$, of the Cauchy stress tensor is decomposed as follows:

> CAG: the liquid is incompressible, but the mixture is compressible, change it

$$\langle\underline{\sigma}^l\rangle = -\langle p^l\rangle\underline{\mathbb{I}} + \langle\underline{\mathbb{S}}^l\rangle \tag{4.5a}$$

$$\langle\underline{\sigma}^l\rangle = -\langle p^l\rangle\underline{\mathbb{I}} + 2\mu^l\langle\underline{\dot{\varepsilon}}^l\rangle + \langle\underline{\tau}^l\rangle \tag{4.5b}$$

where $\langle \underline{\dot{\varepsilon}}^l \rangle$ is the strain rate tensor that depends on the average liquid velocity:

$$\langle \underline{\dot{\varepsilon}}^l \rangle = \underline{\nabla} \langle \vec{v}^l \rangle + \underline{\nabla}^{\mathbf{t}} \langle \vec{v}^l \rangle \tag{4.6}$$

and $\underline{\tau}^l$ is the extra stress tensor in the liquid, given by:

$$\langle \underline{\tau}^l \rangle = -\lambda \nabla \cdot \langle \vec{v}^l \rangle \underline{\mathbb{I}} \tag{4.7a}$$

where λ is a dilatational viscosity **CITE RAP2003**. For an incompressible flow, the divergence term vanishes, hence the classical Newtonian constitutive law is retrieved. In the literature, the coefficient λ is taken proportional to the viscosity: $\lambda = \frac{2}{3} \mu^l$

Formulation

The momentum conservation equation in the liquid writes:

$$\frac{\partial}{\partial t} \left(\rho^l g^l \vec{v}^l \right) + \vec{\nabla} \cdot \left(\rho^l g^l \vec{v}^l \times \vec{v}^l \right) = \vec{\nabla} \cdot \left(g^l \underline{\sigma}^l \right) + g^l \vec{F}_{\mathrm{v}} + \vec{\Gamma}^l \tag{4.8}$$

where $\vec{F}_{\mathrm{v}}$ is an external volume force. The effect of the mass balance obtained in the previous section is incorporated by expanding the temporal and spatial derivatives in the momentum equation, taking firstly the left-hand side of equation (4.8).

$$\text{LHS} = \rho^l \frac{\partial}{\partial t} \left(g^l \vec{v}^l \right) + g^l \vec{v}^l \frac{\partial \rho^l}{\partial t} + \vec{v}^l \nabla \cdot \left(\rho^l g^l \vec{v}^l \right) + \underline{\nabla} \vec{v}^l \left(\rho^l g^l \vec{v}^l \right) \tag{4.9a}$$

$$= \rho^l \underbrace{\frac{\partial}{\partial t} \left(g^l \vec{v}^l \right)}_{\substack{\text{Unsteady} \\ \text{Acceleration}}} + \left(\rho^l - \rho^s \right) \underbrace{\frac{\partial g^s}{\partial t} \vec{v}^l}_{\substack{\text{Shrinkage} \\ \text{Acceleration}}} + \rho^l \underbrace{\underline{\nabla} \vec{v}^l \left(g^l \vec{v}^l \right)}_{\substack{\text{Advective} \\ \text{Acceleration}}} \tag{4.9b}$$

The development in (4.9b) shows that the origin of the flow, namely its acceleration, is attributed to three causes: i) unsteady acceleration: a temporal change of a particle's velocity, ii) shrinkage-induced acceleration: a local "suction" effect at the solid-liquid interface (where $\frac{\partial g^s}{\partial t} > 0$) caused by the density jump $\left(\rho^l - \rho^s \right)$ and iii) convective acceleration: a spatial change in the velocity field. The effect of the *shrinkage-induced* flow is introduced using the mass balance in equation (4.3). The right-hand side of equation (4.8) is now expanded:

$$\text{RHS} = \vec{\nabla} \cdot \left(\langle p^l \rangle \underline{\mathbb{I}} + 2\mu^l \langle \underline{\dot{\varepsilon}}^l \rangle + \langle \underline{\tau}^l \rangle \right) + g^l \rho^l \vec{g} + \vec{\Gamma}_p^l + \vec{\Gamma}_{\mathbb{S}}^l \tag{4.10a}$$

$$= -\vec{\nabla} \left(g^l p^l \right) + \vec{\nabla} \cdot \left(2\mu^l \langle \underline{\dot{\varepsilon}}^l \rangle \right) + \vec{\nabla} \cdot \left(-\frac{2}{3} \mu^l \nabla \cdot \langle \vec{v}^l \rangle \underline{\mathbb{I}} \right) + g^l \rho^l \vec{g} + \vec{\Gamma}_p^l + \vec{\Gamma}_{\mathbb{S}}^l \tag{4.10b}$$

$$= -p^l \vec{\nabla} g^l - g^l \vec{\nabla} p^l + \vec{\nabla} \cdot \left(2\mu^l \langle \underline{\dot{\varepsilon}}^l \rangle \right) + \vec{\nabla} \cdot \left(-\frac{2}{3} \mu^l \nabla \cdot \langle \vec{v}^l \rangle \underline{\mathbb{I}} \right) + g^l \rho^l \vec{g} + \vec{\Gamma}_p^l + \vec{\Gamma}_{\mathbb{S}}^l \tag{4.10c}$$

$$= -g^l \vec{\nabla} p^l + \vec{\nabla} \cdot \left(\mu^l \left(\underline{\nabla} \langle \vec{v}^l \rangle + {}^{\mathbf{t}} \underline{\nabla} \langle \vec{v}^l \rangle \right) \right) + \vec{\nabla} \left(-\frac{2}{3} \mu^l \frac{\rho^l - \rho^s}{\rho^l} \frac{\partial g^s}{\partial t} \right) + g^l \rho^l \vec{g} - g^{l^2} \mu^l \mathbb{K}^{-1} \vec{v}^l \tag{4.10d}$$

The system thus consists of 3 equations (one for each of the components of $\vec{v}^l$) and 4 unknowns ($\vec{v}_x^l$, $\vec{v}_y^l$, $\vec{v}_z^l$ and p). An additional equation is provided by the mass continuity equation (4.3). For convenience, the superficial velocity $\langle \vec{v}^l \rangle$ will be chosen as a velocity unknown instead of the intrinsic average: $\langle \vec{v}^l \rangle = g^l \vec{v}^l$. The final system to solve, after grouping the unknowns in the LHS and the remaining terms in the RHS, is given by:

I changed *split* to *align* here

$$\rho^l \frac{\partial \langle \vec{v}^l \rangle}{\partial t} + \frac{\rho^l - \rho^s}{g^l} \frac{\partial g^s}{\partial t} \langle \vec{v}^l \rangle + \rho^l \underline{\nabla} \vec{v}^l \langle \vec{v}^l \rangle + \vec{\nabla} \cdot \left(2\mu^l \langle \underline{\dot{\varepsilon}}^l \rangle \right) + g^l \mu^l \mathbb{K}^{-1} \langle \vec{v}^l \rangle \tag{4.11}$$

$$= g^l \vec{\nabla} p^l + \vec{\nabla} \left(-\frac{2}{3} \mu^l \nabla \cdot \langle \vec{v}^l \rangle \right) + g^l \rho^l \vec{g} \tag{4.12}$$

$$\nabla \cdot \langle \vec{v}^l \rangle = \frac{\rho^l - \rho^s}{\rho^l} \frac{\partial g^s}{\partial t} \tag{4.13}$$

4.2.3 Energy Conservation

We have seen the averaged energy conservation equation in the case of two phases: a solid phase and an incompressible liquid phase. However, with the incorporation of the shrinkage effect, new terms should appear in the advective-diffusive heat transfer equation.

Assumptions

- The thermal conductivity is constant for both phases: $\langle \kappa \rangle = \langle \kappa^s \rangle = \langle \kappa^l \rangle = \kappa$

- Consequence of the static solid phase: $\langle \rho h \vec{v} \rangle = g^l \rho^l h^l \vec{v}^l + \cancel{g^s \rho^s h^s \vec{v}^s} = g^l \rho^l h^l \vec{v}^l$

- The system's enthalpy may thermodynamically evolve with pressure, knowing that $h = e + \frac{p}{\rho}$, where e is the internal energy and p is the pressure. It infers that the heat transport equation may contain a contribution attributed to volume compression/expansion:

$$\frac{\partial p}{\partial t} + \nabla \cdot \left(p \vec{v} \right) = \frac{\partial p}{\partial t} + p \nabla \cdot \vec{v} + \vec{v} \cdot \vec{\nabla} p \tag{4.14}$$

  In the literature, this contribution has been always neglected, even when accounting for solidification shrinkage, owing to the small variations of pressure.

- Another contribution is also neglected in solidification problems, that is the heat generated by mechanical deformation, $\mathbb{S} : \dot{\varepsilon}$

Formulation

The unknowns in the energy conservation are the average volumetric enthalpy $\langle \rho h \rangle$ and temperature T. The energy conservation equation writes:

$$\frac{\partial \langle \rho h \rangle}{\partial t} + \nabla \cdot \langle \rho h \vec{v} \rangle = \nabla \cdot \left(\langle \kappa \rangle \vec{\nabla} T \right) \tag{4.15a}$$

$$\frac{\partial \langle \rho h \rangle}{\partial t} + \nabla \cdot \left(g^l \rho^l h^l \vec{v}^l \right) = \nabla \cdot \left(\kappa \vec{\nabla} T \right) \tag{4.15b}$$

$$\frac{\partial \langle \rho h \rangle}{\partial t} + \rho^l h^l \nabla \cdot \langle \vec{v}^l \rangle + \langle \vec{v}^l \rangle \cdot \vec{\nabla} \left(\rho^l h^l \right) = \nabla \cdot \left(\kappa \vec{\nabla} T \right) \tag{4.15c}$$

$$\frac{\partial \langle \rho h \rangle}{\partial t} + \cancel{\rho^l} h^l \frac{\rho^l - \rho^s}{\cancel{\rho^l}} \frac{\partial g^s}{\partial t} + \langle \vec{v}^l \rangle \cdot \vec{\nabla} \left(\rho^l h^l \right) = \nabla \cdot \left(\kappa \vec{\nabla} T \right) \tag{4.15d}$$

$$\frac{\partial \langle \rho h \rangle}{\partial t} + \left(\rho^l - \rho^s \right) h^l \frac{\partial g^s}{\partial t} + \langle \vec{v}^l \rangle \cdot \vec{\nabla} \left(\rho^l h^l \right) = \nabla \cdot \left(\kappa \vec{\nabla} T \right) \tag{4.15e}$$

(a) Initial state   **(b)** Solidification onset   **(c)** Final state
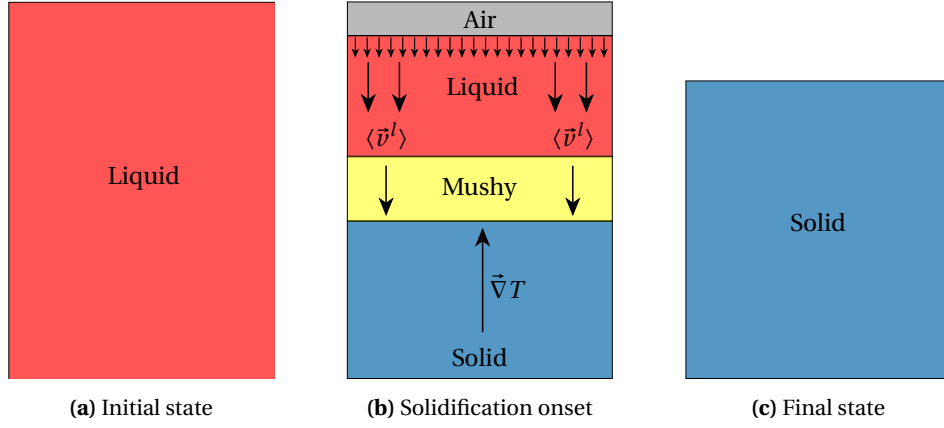
Figure 4.2 Effect of shrinkage flow on a solidifying ingot

$$\frac{\partial \langle \rho h \rangle}{\partial t} + \rho^l \langle \vec{v}^l \rangle \cdot \vec{\nabla} h^l = \nabla \cdot \left(\kappa \vec{\nabla} T \right) + \left(\rho^s - \rho^l \right) h^l \frac{\partial g^s}{\partial t} \qquad (4.16)$$

Discussion

In order to keep things simple, the term "enthalpy" will refer henceforth to "volume enthalpy", otherwise, we will explicitly use the term "mass enthalpy". It is important to understand the meaning of the terms in equation (4.16). The first term in the left-hand side is the temporal change in the system's average enthalpy, i.e. a temporal change in the volume enthalpy of any of the phases in the course of solidification. The second LHS term is a dot product between the superficial liquid velocity and the the gradient of the liquid's enthalpy. Since phase densities are constant in our case, the gradient term reduces to the liquid's mass enthalpy. If we consider a representative volume element (RVE) in the liquid phase, far from the mushy zone, we can stipulate:

$$\vec{\nabla} h^l = C_p^l \vec{\nabla} T \qquad (4.17)$$

assuming that the phase mass specific heat, C_p^l, is constant. Therefore, the liquid enthalpy is advected in the case where the velocity vector is not orthogonal to the temperatre gradient. The advection reaches its maximum when the two vectors have the same direction. Consider, for instance, a filled ingot with a cooling flux applied to its bottom surface. If the density variation with temperature were to be neglected, then the sole mechanical driving force in the melt is the density jump at the solid-liquid interface ahead of the mushy zone. The temperature gradient in such a case is vertical upward, while the velocity vector is in the opposite direction. The advective term writes:

$$\rho^l \langle \vec{v}^l \rangle \cdot \vec{\nabla} h^l = -\rho^l C_p^l \| \langle \vec{v}^l \rangle \| \| \vec{\nabla} T \| \qquad (4.18)$$

We see that the second RHS term in equation (4.16) acts as a heat source at the interface between the the phases, in this particular solidification scenario. Another heat power (of unit $W m^{-3}$) adds to the system within the mushy, that is the second term in the right-hand side of the same equation. This term is proportional to the solidification rate. Finally, the first RHS term accounts for thermal diffusion within the phases.

It should be emphasized that the assumption of a constant specific heat in the liquid in equation (4.17) applies when no macrosegregation occurs. Nonetheless, when the latter is considered, the phases specific and latent heats become highly dependent on the local average composition. It then

advisable to use the thermodynamic tabulation approach, where the enthalpies are directly tabulated as functions of temperature and composition.

4.2.4 Species Conservation

The last conservation principle is applied to the chemical species or solutes. This principle allows predicting macrosegregation when applied to a solidification system, along with the mass, momentum and energy balances. However, the conservation equation should be reformulated in the case of a melt flow driven by shrinkage.

Assumptions

- The alloy is binary, i.e., it is composed from one solute, and hence the notation of the average composition without a solute index: $\langle w \rangle$ for the mass composition and $\langle \rho w \rangle$ for the volume composition

- The solid fration is determined assuming complete mixing in both phases, hence the lever rule is applicable. It should be mentionned that the solidification path in the current approach is tabulated using thermodynamic data at equilibrium

- The solutal diffusion coefficient D^s in the solid phase is neglected in the mass diffusive flux term. The remaining term, D^l, is a mass diffusion coefficient in the liquid phase, of unit $m^2 s^{-1}$

- Consequence of the static solid phase: $\langle \rho w \vec{v} \rangle = g^l \rho^l \langle w \rangle^l \vec{v}^l + \cancel{g^s \rho^s \langle w \rangle^s \vec{v}^s} = g^l \rho^l \langle w \rangle^l \vec{v}^l$

Formulation

The species conservation is pretty similar the energy conservation formluted in the previous section. For a binary alloy, we can write:

$$\frac{\partial \langle \rho w \rangle}{\partial t} + \nabla \cdot \langle \rho w \vec{v} \rangle = \nabla \cdot \left(\rho^l \langle D^l \rangle \vec{\nabla} \langle w \rangle^l \right) \tag{4.19a}$$

$$\frac{\partial \langle \rho w \rangle}{\partial t} + \nabla \cdot \left(g^l \rho^l \langle w \rangle^l \vec{v}^l \right) = \nabla \cdot \left(g^l \rho^l D^l \nabla \langle w \rangle^l \right) \tag{4.19b}$$

$$\frac{\partial \langle \rho w \rangle}{\partial t} + \rho^l \langle w \rangle^l \nabla \cdot \langle \vec{v}^l \rangle + \langle \vec{v}^l \rangle \cdot \vec{\nabla} \left(\rho^l \langle w \rangle^l \right) = \nabla \cdot \left(g^l \rho^l D^l \vec{\nabla} \langle w \rangle^l \right) \tag{4.19c}$$

$$\frac{\partial \langle \rho w \rangle}{\partial t} + \cancel{\rho^l} \langle w \rangle^l \frac{\rho^l - \rho^s}{\cancel{\rho^l}} \frac{\partial g^s}{\partial t} + \langle \vec{v}^l \rangle \cdot \vec{\nabla} \left(\rho^l \langle w \rangle^l \right) = \nabla \cdot \left(g^l \rho^l D^l \vec{\nabla} \langle w \rangle^l \right) \tag{4.19d}$$

$$\frac{\partial \langle \rho w \rangle}{\partial t} + \left(\rho^l - \rho^s \right) \langle w \rangle^l \frac{\partial g^s}{\partial t} + \langle \vec{v}^l \rangle \cdot \vec{\nabla} \left(\rho^l \langle w \rangle^l \right) = \nabla \cdot \left(g^l \rho^l D^l \vec{\nabla} \langle w \rangle^l \right) \tag{4.19e}$$

$$\boxed{\frac{\partial \langle \rho w \rangle}{\partial t} + \rho^l \langle \vec{v}^l \rangle \cdot \vec{\nabla} \langle w \rangle^l = \nabla \cdot \left(\rho^l D^l \vec{\nabla} \langle w \rangle^l \right) + \left(\rho^s - \rho^l \right) \langle w \rangle^l \frac{\partial g^s}{\partial t}} \tag{4.20}$$

Discussion

The species transport equation is usually derived with the volumetric average composition $\langle \rho w \rangle$, then divided by the density, which is constant if no solidification shrinkage occurs. In the case where macrosegregation is solely due to fluid flow generated by natural or forced convection, the overall volume remains constant. It is thus convenient to compute composition variations using the mass

variable $\langle w \rangle$. However, in the current context, the volume is subject to changes, hence the formulation of equation (4.20) with $\langle \rho w \rangle$.

4.3 Test cases

4.3.1 Validation of LS transport

perform test case simulation of buyoancy driven air droplet in water by 2005Nagrath that I also have seen in Shyamprasad's masters report)

I read it quickly without noticing: what time step δt did they use ?

4.3.2 Shrinkage without macrosegregation

Smacs or Pseudo-Smacs test case with Level set and shrinkage

Considerations

Explain how the flow and heat transfer in the air are not important

Model equations

Give the strong form equations to be solved OR simply refer the previous section where the model was defined

Initial and boundary conditions for energy and momentum

Initially we have liquid and air at rest.

Results and discussion

Chapter 5

Macrosegregation with shrinkage and deformable solid OR Application to TEXUS

This chapter will depend on the progress in the shrinkage simulations. If everything goes with shrinkage, then maybe i can put it in Thercast and test the solid deformation also and apply to TEXUS If not then this chapter will only cover these topics:

- What are the CCEMLCC experimental facilities (ground experiments, sound rocket, ISS)

- Focus on TEXUS (setup, conditions, previous results, recent failures...)

-

Conclusion and Perspectives

Conclusions

The summary of what we did in the previous chapters

Future Work

What did we miss in our models that can be potentialy important for the coming years

Appendix A

Notes

from

For many natural-convection flows, you can get faster convergence with the Boussinesq model than you can get by setting up the problem with fluid density as a function of temperature. This model treats density as a constant value in all solved equations, except for the buoyancy term in the momentum equation:

$$(\rho - \rho_0)g \approx -\rho_0 \beta (T - T_0)g \tag{A.1}$$

where ρ_0 is the (constant) density of the flow, T_0 is the operating temperature, and β is the thermal expansion coefficient. Equation 13.2-18 is obtained by using the Boussinesq approximation $\rho = \rho_0(1 - \beta \Delta T)$ to eliminate ρ from the buoyancy term. This approximation is accurate as long as changes in actual density are small; specifically, the Boussinesq approximation is valid when $\beta(T - T_0) \ll 1$.

A.1 Useful Expressions

> address a problem: attend to, apply oneself to, tackle, see to, deal with, confront, come to grips with, get down to, turn one's hand to, take in hand, undertake, concentrate on, focus on, devote oneself to "the selectmen failed to address the issue of subsidies"

- the basic premise = the basic argument is that ...

- A complication inherent in this approach is that

- an important objective of the present study is to

Appendix A. Notes

Bibliography

[**Ahmad et al. 1998**]
Ahmad, N. et al. (1998). "Numerical simulation of macrosegregation: a comparison between finite volume method and finite element method predictions and a confrontation with experiments." *Metallurgical and Materials Transactions A,* 29 (2), pp. 617–630. URL: http://link.springer.com/article/10.1007/s11661-998-0143-9 (cited on page 8).

[**Auburtin et al. 2000**]
Auburtin, P. et al. (2000). "Freckle formation and freckle criterion in superalloy castings." *Metallurgical and Materials Transactions B,* 31 (4), pp. 801–811. URL: http://link.springer.com/article/10.1007/s11663-000-0117-9 (cited on page 18).

[**Beckermann 2002**]
Beckermann, C. (2002). "Modelling of macrosegregation: applications and future needs." *International Materials Reviews,* 47 (5), pp. 243–261 (cited on page 8).

[**Beckermann et al. 2000**]
Beckermann, C. et al. (2000). "Development of a freckle predictor via rayleigh number method for single-crystal nickel-base superalloy castings." *Metallurgical and Materials Transactions A,* 31 (10), pp. 2545–2557. URL: http://link.springer.com/article/10.1007/s11661-000-0199-7 (cited on page 16).

[**Carozzani 2012**]
Carozzani, T. (2012). "Développement d'un modèle 3D Automate Cellulaire-Éléments Finis (CAFE) parallèle pour la prédiction de structures de grains lors de la solidification d'alliages métalliques." PhD thesis. Ecole Nationale Supérieure des Mines de Paris. URL: http://pastel.archives-ouvertes.fr/pastel-00803282 (cited on page 13).

[**Carozzani et al. 2013**]
Carozzani, T. et al. (2013). "Direct Simulation of a Solidification Benchmark Experiment." *Metallurgical and Materials Transactions A,* 44 (2), pp. 873–887. URL: http://link.springer.com/article/10.1007/s11661-012-1465-1 (cited on pages 8, 13, 14).

[**Dantzig et al. 2009**]
Dantzig, J. A. and M. Rappaz (2009). *Solidification.* EPFL Press (cited on pages 2, 13).

Bibliography

[Felicelli et al. 1991]
Felicelli, S. D. et al. (1991). "Simulation of freckles during vertical solidification of binary alloys." *Metallurgical Transactions B,* 22 (6), pp. 847–859. URL: http://link.springer.com/article/10.1007/BF02651162 (cited on page 2).

[Gandin 2000]
Gandin, C. A. (2000). "From constrained to unconstrained growth during directional solidification." *Acta Materialia,* 48 (10), pp. 2483–2501. URL: http://www.sciencedirect.com/science/article/pii/S1359645400000707 (cited on page 12).

[Giamei et al. 1970]
Giamei, A. F. and B. H. Kear (1970). "On the nature of freckles in nickel base superalloys." *Metallurgical Transactions,* 1 (8), pp. 2185–2192. URL: http://link.springer.com/article/10.1007/BF02643434 (cited on page 2).

[Hachani et al. 2012]
Hachani, L. et al. (2012). "Experimental analysis of the solidification of Sn–3 wt.%Pb alloy under natural convection." *International Journal of Heat and Mass Transfer,* 55 (7–8), pp. 1986–1996. URL: http://www.sciencedirect.com/science/article/pii/S0017931011007009 (cited on page 14).

[Hebditch et al. 1974]
Hebditch, D. J. and J. D. Hunt (1974). "Observations of ingot macrosegregation on model systems." *Metallurgical Transactions,* 5 (7), pp. 1557–1564. URL: http://link.springer.com/article/10.1007/BF02646326 (cited on page 14).

[Karagadde et al. 2014]
Karagadde, S. et al. (2014). "3-D microstructural model of freckle formation validated using in situ experiments." *Acta Materialia,* 79, pp. 168–180. URL: http://www.sciencedirect.com/science/article/pii/S1359645414004984 (cited on page 18).

[Ni et al. 1991]
Ni, J. and C. Beckermann (1991). "A volume-averaged two-phase model for transport phenomena during solidification." *Metallurgical Transactions B,* 22 (3), pp. 349–361. URL: http://link.springer.com/article/10.1007/BF02651234 (cited on pages 10, 13).

[Pollock et al. 1996]
Pollock, T. M. and W. H. Murphy (1996). "The breakdown of single-crystal solidification in high refractory nickel-base alloys." *Metallurgical and Materials Transactions A,* 27 (4), pp. 1081–1094. URL: http://link.springer.com/article/10.1007/BF02649777 (cited on page 18).

[Ramirez et al. 2003]
Ramirez, J. C. and C. Beckermann (2003). "Evaluation of a rayleigh-number-based freckle criterion for Pb-Sn alloys and Ni-base superalloys." *Metallurgical and Materials Transactions A,* 34 (7), pp. 1525–1536. URL: http://link.springer.com/article/10.1007/s11661-003-0264-0 (cited on page 17).

[Rappaz et al. 2003]

Rappaz, M. et al. (2003). *Numerical Modeling in Materials Science and Engineering.* Springer Series in Computational Mathematics. Springer Berlin Heidelberg (cited on page 10).

[Rivaux 2011]

Rivaux, B. (2011). "Simulation 3D éléments finis des macroségrégations en peau induites par déformations thermomécaniques lors de la solidification d'alliages métalliques." PhD thesis. École Nationale Supérieure des Mines de Paris. URL: http://pastel.archives-ouvertes.fr/pastel-00637168 (cited on pages 3, 13).

[Shevchenko et al. 2013]

Shevchenko, N. et al. (2013). "Chimney Formation in Solidifying Ga-25wt pct In Alloys Under the Influence of Thermosolutal Melt Convection." *Metallurgical and Materials Transactions A,* 44 (8), pp. 3797–3808. URL: http://link.springer.com/article/10.1007/s11661-013-1711-1 (cited on page 18).

[Yuan et al. 2012]

Yuan, L. and P. D. Lee (2012). "A new mechanism for freckle initiation based on microstructural level simulation." *Acta Materialia,* 60 (12), pp. 4917–4926. URL: http://www.sciencedirect.com/science/article/pii/S1359645412003205 (cited on page 18).